Laser Photonics Rev. **7,** No. 6, 1043–1048 (2013) / **DOI** 10.1002/lpor.201300087

LASER & PHOTONICS REVIEWS

Abstract In this article a monolithic resonant terahertz sensor element with a noise equivalent power superior to that of typical commercial room temperature single pixel terahertz detectors and capable of close to real time read-out rates is presented. The detector is constructed via the integration of a metamaterial absorber and a micro-bolometer sensor. An absorption magnitude of 57% at 2.5 THz, a minimum NEP of 37 pW/$\sqrt{Hz}$ and a thermal time constant of 68 ms for the sensor are measured. As a demonstration of detector capability, it is employed in a practical Nipkow terahertz imaging system. The monolithic resonant terahertz detector is readily scaled to focal plane array formats by adding standard read-out and addressing circuitry enabling compact, low-cost terahertz imaging.

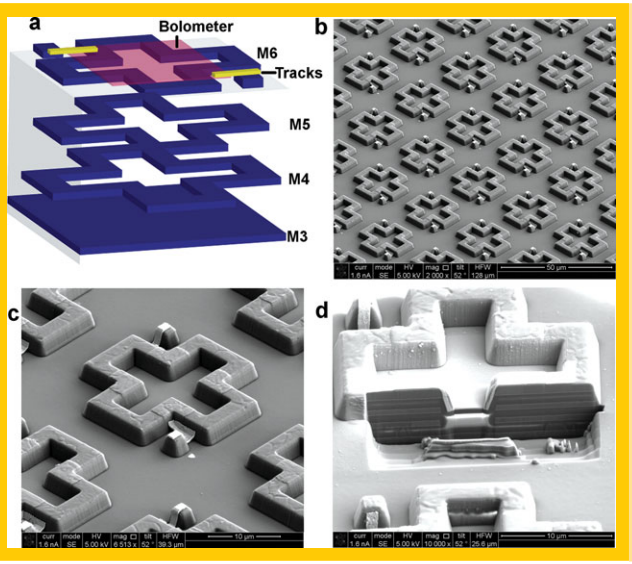

ORIGINAL PAPER

A monolithic resonant terahertz sensor element comprising a metamaterial absorber and micro-bolometer

James Grant[1,*], Ivonne Escorcia-Carranza[1], Chong Li[1], Iain J. H. McCrindle[1], John Gough[2], and David R. S. Cumming[1]

1. Introduction

Advancements in the field of terahertz (THz) science and technology have resulted in a number of important applications including security and medical imaging [1], explosive detection [2,3], non-destructive testing [4] and wireless communication [5]. Research has been driven by the unique properties of THz radiation: it is non-ionising thus safe to biological tissue; transparent to several common plastics and fibres; and has a shorter wavelength than millimeter waves, giving a higher spatial resolution. In addition several materials, such as explosives and illicit drugs, have characteristic THz spectroscopic signatures that can be readily identified [6].

The proliferation of these applications into everyday life has been hampered by the lack of inexpensive, compact and room-temperature THz sources and detectors. In this work we focus on the development of a detector targeting single frequency terahertz imaging applications such as stand-off security and non-invasive package inspection. State-of-the-art commercial THz detectors for imaging applications are typically comprised of discrete components that are bulky and exhibit a low level of integration at high cost. Common THz detectors include pyroelectric sensors [7], Schottky barrier diodes [8] and field-effect transistors [9]. However these detectors have one or more limitations such as low sensitivity, slow speed, the requirement for cryogenic cooling and the difficulty of scaling to array formats required for THz imaging. Most THz images today are built up one pixel at a time, through raster scanning with single-point detectors [10]. Linear arrays of discrete detectors based on superconducting tunnel junctions [11] and niobium nitride micro-bolometers [12] coupled with scanning optics do offer the advantage of faster image acquisition speed compared to single pixel counterparts. Uncooled two dimensional IR focal plane arrays (FPAs) have been used in THz imaging experiments, but the detection efficiency is less than 5% [13]. Efforts have been made to optimise uncooled IR FPAs for the THz frequency regime by implementing antenna structures of appropriate geometry for the THz waveband coupled to various sensor elements such as amorphous silicon [14], vanadium oxide [15] and niobium [16]. Imaging experiments with such antenna coupled micro-bolometer arrays fabricated on top of CMOS chips and with a photoconductive antenna source show promising results [17]. Complementary metal-oxide semiconductor

[1] Microsystems Technology Group, School of Engineering, University of Glasgow, G128LT, UK
[2] Texas Instruments, Greenock, PA16 0EQ, UK
*Corresponding author: e-mail: james.grant@glasgow.ac.uk

(CMOS) transistors are also capable of detecting THz radiation and noise equivalent powers of 470 $pW/\sqrt{Hz}$ at 0.9 THz have been demonstrated [18], however above this frequency the detection efficiency drops off markedly [19]. We aim to develop pixel technology for use at frequencies well above 1.0 THz.

The lack of natural frequency selective materials that absorb THz radiation has prompted researchers to explore artificial means such as the use of metamaterial (MM) devices [20]. MMs are arrays of sub-wavelength elements, the structure of which, rather than their composition, dictates their electromagnetic properties. Applications include cloaking [21], superlensing [22] and plasmonically induced transparency [23]. MMs can also be used to create resonant absorber structures where the radiation is absorbed in a device thickness of $< \lambda/30$, overcoming the thickness limitation of traditional quarter wavelength devices [24–26]. Single band, dual band and broadband absorbers have been demonstrated across the THz frequency range [24, 27, 28] however until now such absorbers have not been integrated with a sensing element and used in a practical THz imaging experiment. An 11 × 11 MM based focal plane array detector operating in the S band (2–4 GHz) has been presented [29] whereby the associated read-out electronics are discrete and implemented on a printed circuit board. In our approach we realise the periodic metamaterial array in a silicon chip containing the front end readout electronics. The approach is feasible in the THz range, since the required array dimensions are compatible with CMOS foundry processes. In this article we experimentally demonstrate a monolithic resonant THz detector constructed via the integration of a resonant MM absorber with a micro-bolometer sensor. Moreover, the MM absorber component of our monolithic resonant detector is made directly in the metallic and oxide layers available in a standard 0.18 μm CMOS process (CMOS9T5V Texas Instruments). As a demonstration of the detector capability we use the device in a THz transmission imaging experiment based on a Nipkow disk. The approach to detecting THz radiation and the natural scalability to large array formats presented here is a significant advance toward compact, low-cost and real-time THz imaging systems.

2. Design considerations and spectral response characteristics of the monolithic resonant terahertz detector

A 3D schematic diagram depicting the unit cell of our MM based monolithic resonant terahertz detector is shown in Fig. 1a. The pixel consists of two elements; the MM absorber and the micro-bolometer sensor. Three cross shaped electric ring resonators (ERRs) are stacked on top of a continuous metallic ground plane, separated by an insulating layer (SiO_2) to form a broadband MM absorber. A micro-bolometric sensor is patterned on top of the MM absorber structure and Ti/Al tracks defined to connect the sensor to the M6 studs. The metal and inter-metal dielectric thicknesses of the CMOS layers are proprietary however the other geometric parameters of the structure are as follows: bolometer thickness = 300 nm, Ti/Au tracks thickness = 1000 nm, M6 cross arm length = 22.5 μm, M5 cross arm length = 23.5 μm, M4 cross arm length = 24.5 μm and cross arm width = 2.5 μm. To reduce the thermal mass of the pixel and thus improve the detector responsivity, the underlying silicon beneath the pixel is removed using a standard silicon plasma etching technique. Scanning electron microscope (SEM) images of a section of the array and of a single pixel are shown in Fig. 1b and Fig. 1c respectively.

Our previous studies [26] have shown that the insulating layer properties; namely the thickness, refractive index and loss component, between the ground plane and the ERR, have a significant effect on the absorption magnitude. THz MM absorbers to date have been fabricated in research facilities where the insulating layer thickness can be easily tuned however in our case the thickness of the insulating layer, namely the intermetal-dielectric (nominally SiO_2), is fixed by the CMOS foundry process. Moreover the refractive index and loss component of the CMOS inter-metal dielectric layers are not well known at THz frequencies. These facts coupled with the observation that MM based absorption is inherently narrowband (FWHM typically less than 20% the centre frequency) present a significant challenge when designing a MM device to operate at a specific frequency. In our work we use a CO_2 laser pumped methanol vapour laser operating at 2.52 THz. We therefore require the MM device to strongly absorb the same frequency. Therefore, to maximise the likelihood of attaining strong absorption in the region of 2.5 THz, three stacked ERRs are employed to broaden the absorption spectrum. Stacking ERRs on top of a continuous ground plane has been shown to improve the FWHM to ∼48% of the centre frequency [28]. A cross-sectional SEM image of the MM absorber pixel, clearly showing the three metallic ERRs and metallic ground plane, is shown in Fig. 1d.

The optimised MM absorber structure was designed using 3D finite difference time domain (FDTD) simulations (Lumerical Inc. [30]). The 3D simulations were performed with a plane wave source incident in the z direction of the unit cell. Periodic boundary conditions were used for the x and y boundaries and perfectly matched layers employed for the z direction boundaries. The mesh step size around the monolithic resonant terahertz detector was $\Delta x = \Delta y = 0.1$ μm and $\Delta z = 0.05$ μm. The unit cell period was 30 μm by 30 μm. The metallic sections of the absorber were modelled as Al with a frequency independent conductivity of 4×10^7 Sm^{-1} while the inter-metal dielectric regions were modelled using SiO_2 Palik from the Lumerical software database. Reflection and transmission spectra were calculated at planes z = 100 μm and z = −100 μm. Due to the inherent symmetry of the MM absorber device the FDTD simulations revealed the spectral absorption characteristics were not sensitive to the polarisation angle of the incident EM wave.

Figure 2a shows the simulated spectral characteristics for the three ERR absorber device and for a single M6

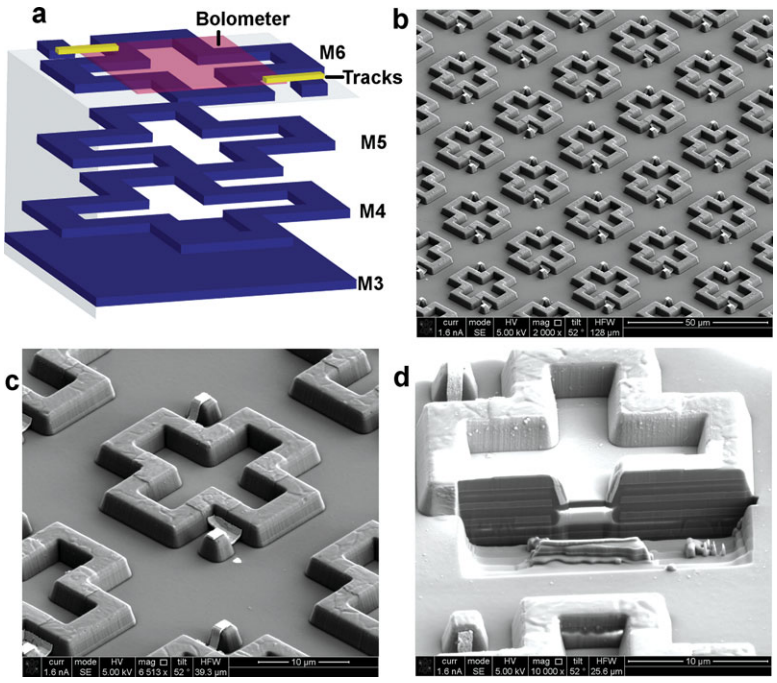

Figure 1 a) 3D schematic diagram of the monolithic resonant terahertz detector. b) and c) show scanning electron micrographs of a section of the array and of a single pixel respectively after post-processing of the CMOS chip by depositing the vanadium oxide sensor element and Ti/Au connecting tracks. In c), the sputtered vanadium oxide film follows the topography of the M6 ERR as a single film. d) Cross-sectional scanning electron micrographs of a single pixel revealing the three ERR metallic layers and the metallic ground plane. A focused ion beam was used to mill the square trench.

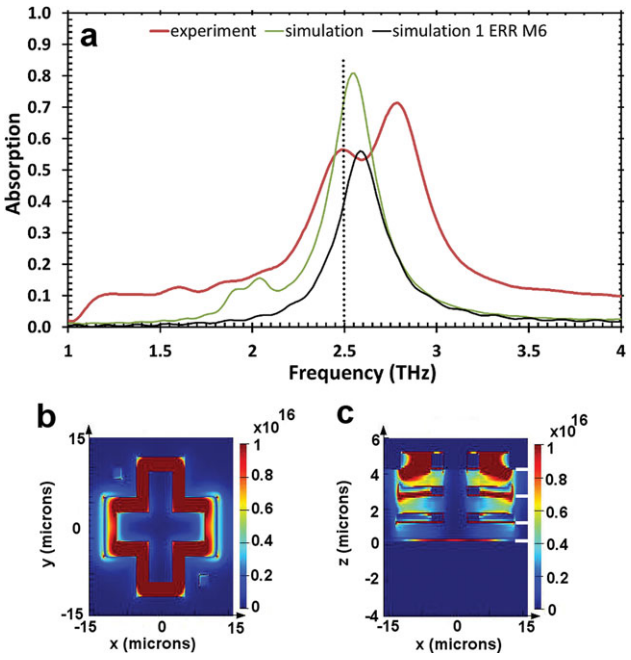

Figure 2 a) Experimental (red) and simulated (green) spectral response curves of the monolithic resonant THz detector. For comparison the simulated spectral response of a single ERR in M6 is also shown (black). b) simulated absorption distribution in the x-y plane at the bottom of M6 and c) simulated x-z absorption distribution plot at y = 5 μm. The solid white lines in c) denote the bottom of the metallic layers.

ERR absorber. The single M6 absorber has a narrow absorption peak at 2.56 THz and an absorption magnitude of 55%. In contrast, the three layer ERR structure has a broad absorption peak of magnitude 80% at 2.56 THz while at 2.52 THz, our frequency of interest, the absorption magnitude is 78%. Complete post-processed devices were experimentally characterized under vacuum in a Bruker IFS 66v/S Fourier Transform Infrared Spectrometer in transmission mode at normal incidence and in reflection mode at 30° incidence. The measured transmission spectra were normalized with respect to the signal measured from a 4 mm diameter open aperture and the reflection spectra were normalized to that of a gold mirror. The resulting absorption, A, was therefore calculated using $A(\omega) = 1 - R(\omega) - T(\omega)$ where R is the reflection coefficient and T the transmission coefficient. As the thickness of the ground plane is much greater than the typical skin depth in the THz regime the reflection is the only factor limiting absorption.

The experimental spectrum has two resonance peaks at 2.5 THz and 2.81 THz of magnitude 57% and 70% respectively. Overall there is reasonable agreement between the experimental and simulation spectra. The deviation between the curves can be attributed to several factors; the most significant two are the possibility of a discrepancy in the real and assumed value of the inter-metal dielectric refractive index and potential thickness non-uniformity of the three inter-metal dielectric layers.

To understand the origin of the spectral characteristics, the simulated absorption distributions in the x-y plane at the top of the M6 ERR and in the x-z plane at y = 5 μm at the resonance frequency of 2.52 THz are plotted in Fig. 2b and Fig. 2c respectively. The plots reveal that the regions of maximum absorption occur in the metal layers and also in the first few hundred nanometres of inter-metal dielectric immediately beneath the M6 ERR. These simulation results validate our decision to locate the thermal sensing element directly above the uppermost ERR.

3. CMOS post-processing details and determination of detector noise equivalent power

On receiving the CMOS chips from the foundry three post-processing steps were necessary: (1) deposition of a suitable sensor material, (2) definition of the connecting tracks from the M6 studs to the micro-bolometer element and (3) etching of silicon underneath the bolometer to leave a membrane structure. We chose vanadium oxide (VOx) as the sensor material due its high temperature coefficient of resistance (TCR) and relatively mature deposition technology. A 50 nm Si_3N_4 layer separates the MM absorber from the vanadium oxide resistive micro-bolometer. The 300 nm thick VOx film was deposited at room temperature using RF reactive sputtering of vanadium metal in an oxygen environment. Ti/Au tracks are then added to connect the micro-bolometer to the M6 studs that lead to bond pads. Backside photolithography was used to pattern a circular window of radius 1 mm and the underlying silicon was removed using a standard etch process to make a membrane and minimise the thermal capacitance of the structure. In this prototype chip only 4 pixels were directly connected to bond pads for further characterisation. These 4 pixels were scattered throughout the array and the minimum distance between them was 0.5 mm.

Various figures of merit exist for determining the performance of micro-bolometer sensors. The most commonly used are the responsivity, noise equivalent power (NEP) and thermal time constant. The responsivity can be expressed using the following relation [31]:

$$R_V = \frac{\alpha \eta R I_B}{G_{th}\sqrt{1+\omega^2\tau^2}} \tag{1}$$

where α is the temperature coefficient of resistance, η is the absorption magnitude, R is the resistance of the micro-bolometer, I_B is the bias current, G_{th} is the thermal conductance, ω is the angular chopping modulation frequency and τ is the thermal time constant. The NEP per square root unit bandwidth can be found from the responsivity using the relationship [31]:

$$NEP = \frac{V_N}{R_V} \tag{2}$$

where V_N is the rms noise voltage per square root unit bandwidth of the micro-bolometer element. The main sources of noise in a micro-bolometer sensor are 1/f, Johnson and phonon [31].

To establish the sensor TCR, an environmental chamber in conjunction with a Keithley 4200-SCS Parameter Analyser was used to evaluate the micro-bolometer resistance at temperatures between 10°C and 80°C. At 20°C the measured TCR is −2.49%/K and the micro-bolometer resistance is 17.32 MΩ. The responsivity and thermal time constant of the THz detector were directly determined as follows. The terahertz source was a CO_2 pumped methanol vapour laser (Edinburgh Instruments) operating at 2.52 THz

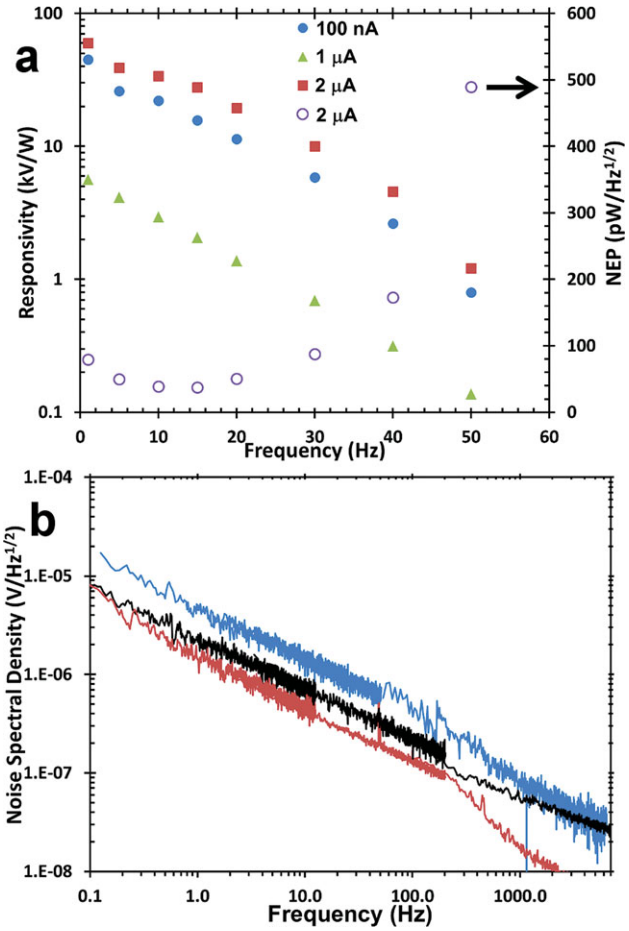

Figure 3 a) Responsivity versus frequency data for bolometer bias currents of 100 nA, 1 μA and 2 μA (closed symbols). NEP data at 2 μA (open symbols) bias is also shown. b) noise spectral density plot at a bias of 100 nA (red line), 1 μA (black line) and 2 μA (blue line).

with a maximum output power of 150 mW. A Tsurpurica lens with a focal length of 10 cm focused the beam down to a diameter of ∼2 mm. The beam shape at the focus position was measured using a commercial IR focal plane array (FLIR). A Scientech AC2500 power meter was used to measure the power at the focus and determine the power incident on each 30 μm × 30 μm pixel. The monolithic resonant THz detector was mounted on an x-y-z stage and positioned at the focus point. A mechanical chopper (Thor Labs) was placed in front of the lens to modulate the THz beam. The micro-bolometer was DC current biased using the Keithley 4200-SCS and the voltage signal detected by a lock-in amplifier (EG&G Model 5210) synchronized to the beam chopper.

Figure 3a shows the measured responsivity of the monolithic resonant terahertz detector with respect to THz modulation frequency from 1 to 50 Hz at 1 atmosphere for several different bias currents. As implied by Eq. (1) the detector responsivity increases with increasing bias current. The DC responsivity and the thermal time constant values of the detector are extracted as 72 kV/W and 68 ms at a

bias current of 2 μA. Figure 3b shows the measured noise spectral density of the monolithic resonant THz detector at bias currents of 100 nA, 1 μA and 2 μA. The measurement set up consists of an Agilent 35670A dynamic signal analyzer, Keithley 4200-SCS current source, a Faraday cage and the detector. The noise spectrum reveals that the dominant noise source is 1/f in nature. In addition the noise increases with increasing bias current. It has been reported that the 1/f noise of VOx films is extremely sensitive to the deposition technique and film stoichiometry [32]. Figure 3a also shows the NEP between 1 Hz and 50 Hz for a bias current of 2 μA. The minimum NEP of 37 $pW/\sqrt{Hz}$ occurs at 15 Hz and steadily increases for higher frequencies. The NEP value is lower than that of current state of the art THz detectors that operate at room temperature such as Schottky diodes [33], pyroelectric devices [34] and field-effect transistors [35], while the extracted thermal time constant of 68 ms is short enough to allow imaging at frame rates of 10 Hz.

4. Nipkow based terahertz imaging experiment using the monolithic terahertz detector

As a practical demonstration of the capability of the monolithic resonant detector we employed it in a Nipkow based THz transmission imaging experiment. The Nipkow disk has been used for imaging systems since the first television was invented in 1929 [36]. The technique is almost 100 years old although it is still used in various modern imaging instruments such as the optical confocal microscope [37]. The experimental set-up is shown in Fig. 4a and is based on a similar approach described by Ma et al. [38]. However, in the present work the apertures in the disk were replaced by Fresnel lenses fabricated in a 100 mm silicon wafer. Each lens is a16-level binary phase shifting diffractive optic with a diameter of 10 mm and a focal length of 5.5 cm [39]. The lenses in the disk are positioned in the form of a single-turn spiral starting from an external radial point of the disk and proceeding to the centre. The Fresnel lens is scanned across the incident 15 mm diameter Gaussian laser beam, sampling a small portion as it moves. The sampled portion is focused into a diameter of 0.7 mm, onto the object. As the disk rotates, the same Fresnel lens travels in a spiral pattern and interrogates a different portion of the object, giving rise to a line scan. Each lens in turn contributes to a new line-scan hence a 2D image is created. When an object is positioned at the image plane, each focused beam behaves as a probe and scans the object sequentially in both the x (radial) and y (rotational) directions. Only 1 lens samples the incident 15 mm beam at any time. In our experiment the object is a 10 mm × 10 mm T shape cut out of a sheet of aluminium (see Fig. 4b) The transmitted beam is reflected and re-focused by a 90° off axis parabolic mirror onto the monolithic resonant THz detector. A mechanical chopper is placed in front of the detector to modulate the THz beam. The same current bias and lock-in detection method, as

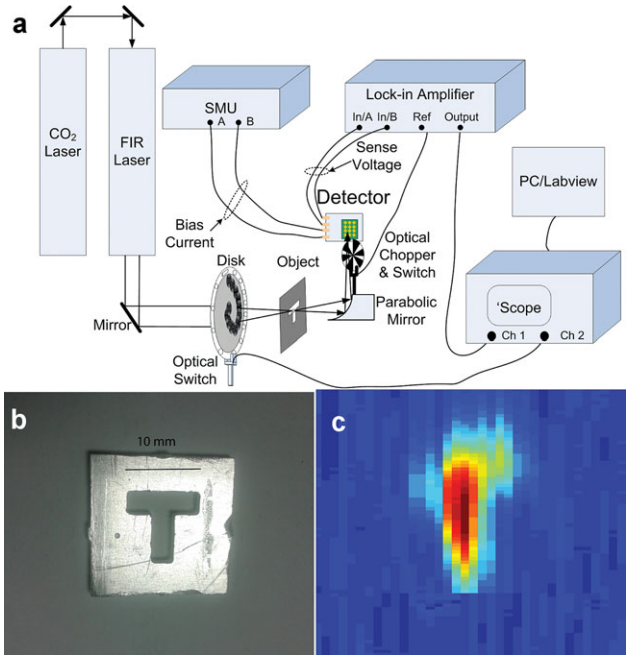

Figure 4 a) Experimental set up for the imaging system based on a Nipkow disk. b) optical image of the cut out "T" shape in aluminum used in the THz imaging experiment. c) THz image taken using the monolithic resonant THz detector.

before, is used. Both the lock-in signal and the timing signal are monitored on a digital oscilloscope. A Labview (National Instruments) program is used to acquire data from the oscilloscope, process the raw data and consequently build a 2-D image using the processed data. Figure 4c shows the captured image using the monolithic resonant THz detector for a bias current of 450 nA, modulation frequency of 1 Hz, lock-in amplifier time constant of 300 ms and a disk rotation speed of 0.2 rpm.

5. Summary

To conclude, a monolithic resonant THz detector, constructed via the combination of a MM absorber with a micro-bolometer sensor element is presented. The absorber is realised directly in the layers of a standard 0.18 μm CMOS process and the micro-bolometer sensor element is defined by post-processing procedures. Numerical simulations were performed to design a structure that strongly absorbed at 2.5 THz, the operating frequency of our source. The spectral response, responsivity, thermal time constant and noise characteristics of the detector were experimentally assessed. We demonstrated the capability of the monolithic resonant THz detector in a practical THz imaging experiment based on a Nipkow disk. The presented single pixel device is readily extendable to focal plane array image formats by adding appropriate circuitry. Furthermore, MM absorbers are extremely flexible in that their operating frequency can be scaled simply by modifying the unit cell size, ERR dimensions and insulating layer thickness between the

ERR and the ground plane. The results demonstrate a significant advance toward compact, low-cost real-time THz imaging systems.

Acknowledgements. This work is supported by the Engineering and Physical Sciences Research Council grant numbers EP/I017461/1 and EP/J018678/1. We wish to acknowledge the contribution of the staff and facilities of the James Watt Nanofabrication Centre at Glasgow University and Texas Instruments for provision of CMOS fabrication.

Received: 25 June 2013, **Revised:** 5 August 2013,
Accepted: 19 August 2013

Published online: 10 September 2013

Key words: Imaging, metamaterial, resonant, sensor, terahertz.

References

[1] R. M. Woodward, V. P. Wallace, R. J. Pye, B. E. Cole, D. D. Arnone, E. H. Linfield, and M. Pepper, J Invest Dermatol **120**, 72–78 (2003).
[2] C. Baker, T. Lo, W. R. Tribe, B. E. Cole, M. R. Hogbin, and M. C. Kemp, Proceedings of the IEEE **95**, 1559–1565 (2007).
[3] H. B. Liu, Y. Q. Chen, G. J. Bastiaans, and X. C. Zhang, Opt Express **14**, 415–423 (2006).
[4] K. Kawase, Y. Ogawa, Y. Watanabe, and H. Inoue, Opt Express **11**, 2549–2554 (2003).
[5] J. Federici and L. Moeller, J Appl Phys **107** (2010).
[6] C. J. Strachan, P. F. Taday, D. A. Newnham, K. C. Gordon, J. A. Zeitler, M. Pepper, and T. Rades, J Pharm Sci-Us **94**, 837–846 (2005).
[7] A. Dobroiu, M. Yamashita, Y. N. Ohshima, Y. Morita, C. Otani, and K. Kawase, Appl. Opt. **43**, 5637–5646 (2004).
[8] S. Sankaran and K. K. O, Electron Device Letters, IEEE **26**, 492–494 (2005).
[9] A. Lisauskas, W. von Spiegel, S. Boubanga-Tombet, A. El Fatimy, D. Coquillat, F. Teppe, N. Dyakonova, W. Knap, and H. G. Roskos, Electron Lett **44**, 408–409 (2008).
[10] P. U. Jepsen, D. G. Cooke, and M. Koch, Laser & Photonics Reviews **5**, 124–166 (2011).
[11] S. Ariyoshi, C. Otani, A. Dobroiu, H. Matsuo, H. Sato, T. Taino, K. Kawase, and H. M. Shimizu, Conference Digest of the 2006 Joint 31st International Conference on Infrared and Millimeter Waves and 14th International Conference on Terahertz Electronics, 395–395 (2006).
[12] A. Luukanen, L. Gronberg, P. Helisto, J. S. Penttila, H. Seppa, H. Sipola, C. R. Dietlein, and E. N. Grossman, Terahertz for Military and Security Applications IV **6212**, Y2120–Y2120 (2006).
[13] A. W. M. Lee, B. S. Williams, S. Kumar, Q. Hu, and J. L. Reno, Ieee Photonic Tech L **18**, 1415–1417 (2006).
[14] D. T. Nguyen, F. Simoens, J. L. Ouvrier-Buffet, J. Meilhan, and J. L. Coutaz, Ieee T Thz Sci Techn **2**, 299–305 (2012).
[15] L. Marchese, M. Bolduc, B. Tremblay, M. Doucet, H. Oulachgar, L. Le Noc, F. Williamson, C. Alain, H. Jerominek, and A. Bergeron, Terahertz Physics, Devices, and Systems Iv: Advanced Applications in Industry and Defense **7671** (2010).
[16] S. Cibella, M. Ortolani, R. Leoni, G. Torrioli, L. Mahler, J. H. Xu, A. Tredicucci, H. E. Beere, and D. A. Ritchie, Appl Phys Lett **95** (2009).
[17] J. Oden, J. Meilhan, J. Lalanne-Dera, J. F. Roux, F. Garet, J. L. Coutaz, and F. Simoens, Opt Express **21**, 4817–4825 (2013).
[18] H. Sherry, J. Grzyb, Z. Yan, R. Al Hadi, A. Cathelin, A. Kaiser, and U. Pfeiffer, "A 1kpixel CMOS camera chip for 25fps real-time terahertz imaging applications," in *Solid-State Circuits Conference Digest of Technical Papers (ISSCC)*, 2012 IEEE International, 252–254 (2012).
[19] A. Lisauskas, S. Boppel, V. Krozer, and H. G. Roskos, 2011 Ieee Sensors, 55–58 (2011).
[20] M. Tonouchi, Nat Photonics **1**, 97–105 (2007).
[21] D. Schurig, J. J. Mock, B. J. Justice, S. A. Cummer, J. B. Pendry, A. F. Starr, and D. R. Smith, Science **314**, 977–980 (2006).
[22] N. Fang and X. Zhang, Appl Phys Lett **82**, 161–163 (2003).
[23] T. W. Ebbesen, H. J. Lezec, H. F. Ghaemi, T. Thio, and P. A. Wolff, Nature **391**, 667–669 (1998).
[24] N. I. Landy, C. M. Bingham, T. Tyler, N. Jokerst, D. R. Smith, and W. J. Padilla, Phys Rev B **79**, 125104 (2009).
[25] D. Y. Shchegolkov, A. K. Azad, J. F. O'Hara, and E. I. Simakov, Phys Rev B **82**, 205117 (2010).
[26] J. Grant, Y. Ma, S. Saha, L. B. Lok, A. Khalid, and D. R. S. Cumming, Opt. Lett. **36**, 1524–1526 (2011).
[27] Y. Ma, Q. Chen, J. Grant, S. C. Saha, A. Khalid, and D. R. S. Cumming, Opt. Lett. **36**, 945–947 (2011).
[28] J. Grant, Y. Ma, S. Saha, A. Khalid, and D. R. S. Cumming, Opt. Lett. **36**, 3476–3478 (2011).
[29] D. Shrekenhamer, W. R. Xu, S. Venkatesh, D. Schurig, S. Sonkusale, and W. J. Padilla, Phys Rev Lett **109** (2012).
[30] Lumerical, "Lumerical FDTD" (http://www.lumerical.com/tcad-products/fdtd/), retrieved http://www.lumerical.com/tcad-products/fdtd/.
[31] D. S. P. Kruse, *Uncooled Infrared Imaging Arrays and Systems*, Semiconductors and Semimetals Academic Press, (1997), Vol. 47.
[32] F. Niklaus, C. Vieider, and H. Jakobsen, Proc. SPIE 6836, MEMS/MOEMS Technologies and Applications III, 68360D–68360D (2007).
[33] J. L. Hesler and T. W. Crowe, 2007 Joint 32nd International Conference on Infrared and Millimeter Waves and 15th International Conference on Terahertz Electronics, Vols 1 and 2, 827–828 (2007).
[34] Microtech, "Microtech Pyroelectric Detector Datasheet".
[35] R. Al Hadi, H. Sherry, J. Grzyb, Z. Yan, W. Forster, H. M. Keller, A. Cathelin, A. Kaiser, and U. R. Pfeiffer, IEEE Journal of Solid-State Circuits **47**, 2999–3012 (2012).
[36] J. L. Baird patent, "Apparatus for transmitting views or images to a distance" (1929).
[37] D. M. Grant, D. S. Elson, D. Schimpf, C. Dunsby, J. Requejo-Isidro, E. Auksorius, I. Munro, M. A. Neil, P. M. French, E. Nye, G. Stamp, and P. Courtney, Opt. Lett. **30**, 3353–3355 (2005).
[38] Y. Ma, J. Grant, S. Saha, and D. R. S. Cumming, Opt. Lett. **37**, 1484–1486 (2012).
[39] E. D. Walsby, S. Wang, J. Xu, T. Yuan, R. Blaikie, S. M. Durbin, X. C. Zhang, and D. R. S. Cumming, J Vac Sci Technol B **20**, 2780–2783 (2002).